International Journal of Applied Earth Observations and Geoinformation 101 (2021) 102358

Contents lists available at ScienceDirect

International Journal of Applied Earth Observations and Geoinformation

journal homepage: www.elsevier.com/locate/jag

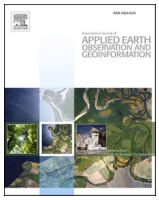

UAV-based individual shrub aboveground biomass estimation calibrated against terrestrial LiDAR in a shrub-encroached grassland

Yujin Zhao [a,1], Xiaoliang Liu [a,e,1], Yang Wang [a], Zhaoju Zheng [d], Shuxia Zheng [a], Dan Zhao [c], Yongfei Bai [a,b,*]

[a] State Key Laboratory of Vegetation and Environmental Change, Institute of Botany, Chinese Academy of Sciences, 20 Nanxincun, Xiangshan 100093, Beijing, China
[b] Colleage of Resources and Environment, University of Chinese Academy of Sciences, Beijing 100049, China
[c] State Key Laboratory of Remote Sensing Science, Aerospace Information Research Institute, Chinese Academy of Sciences, Beijing 100101, China
[d] Remote Sensing Laboratories, Department of Geography, University of Zurich, Zurich CH-8057, Switzerland
[e] State Key Laboratory of Resources and Environmental Information System, Institute of Geographic Sciences and Natural Resources Research, Chinese Academy of Sciences, Beijing 100101, China

ARTICLE INFO

Keywords:
Shrub encroachment
Biomass
Unmanned aerial vehicle (UAV)
Terrestrial laser scanning
Volume
Individual shrub identification

ABSTRACT

Shrub encroachment is an important ecological issue that is increasingly receiving global attention in arid and semiarid grasslands. Monitoring the spatial distribution of encroached shrub aboveground biomass (AGB) is critical for ecological conservation and adaptive ecosystem management. However, the low stature and fine spatial heterogeneity of encroached shrub communities increase difficulties for coarse spatial-resolution satellite images to adequately capture detailed characteristics of individual shrubs. Unmanned aerial vehicle (UAV) can acquire centimeter-level optical images or high-density LiDAR point cloud data, providing an effective means to map encroached shrub AGB spatially explicitly, even at the individual scale. In this study, we first extracted the individual shrubs based on thresholds in normalized difference vegetation index (NDVI) and canopy height model (CHM) using UAV-based multispectral and LiDAR data. For each shrub, we then derived and determined the dominant geometric, spectral, and textural features from the high-resolution multispectral image and the volumetric features from the LiDAR data as predictors of shrub AGB. Finally, we compared the capability of different data sources (UAV-based multispectral image, LiDAR, and their combination) and regression methods (multiple linear, random forest, and support vector regression) to estimate and map the individual shrub AGB in the study area. The volume-based approaches to individual shrub AGB, including global convex hull method, voxel method, and surface differencing method, were also employed using terrestrial laser scanning (TLS) to further calibrate the UAV-based estimation. Our results show that individual shrubs can be accurately extracted based on the threshold method with an overall classification accuracy of 91.8%. The UAV-based AGB estimation suggests that the textural feature, the sum of contrast metric within the individual shrub canopy, is the most important predictor of individual shrub AGB, followed by volumetric, geometric and spectral features. Moreover, the high-resolution multispectral image shows greater potential ($R^2 = 0.83$, RMSE = 106.46 g) than LiDAR ($R^2 = 0.77$, RMSE = 123.33 g) in the estimation of individual shrub AGB, and their combination can only slightly improve the estimation accuracy ($R^2 = 0.86$, RMSE = 101.97 g). Our results also show that TLS-derived volume based on the surface differencing method obtained the best prediction accuracy of individual shrub AGB ($R^2 = 0.91$, RMSE = 79.98 g), and can be used as an alternative of destructive harvesting. This study provides a new insight for quantifying and mapping individual shrub AGB using UAV-based optical sensors and TLS without destructive harvesting in arid and semiarid grasslands.

* Corresponding author at: State Key Laboratory of Vegetation and Environmental Change, Institute of Botany, Chinese Academy of Sciences, 20 Nanxincun, Xiangshan 100093, Beijing, China.
E-mail address: yfbai@ibcas.ac.cn (Y. Bai).
[1] These authors contributed equally to this paper.

https://doi.org/10.1016/j.jag.2021.102358
Received 29 October 2020; Received in revised form 30 April 2021; Accepted 2 May 2021
Available online 12 May 2021

1. Introduction

Shrub encroachment, defined as an increase of coverage, density or biomass of woody plants at the expense of perennial grasses, is a critical ecological issue of increasing global concern in arid and semiarid grasslands (Eldridge et al., 2011; Van Auken, 2009). Due to climate warming, overgrazing, nitrogen deposition and atmospheric CO_2 increases, shrub encroachment shows a widespread expansion into arid and semiarid grasslands worldwide, especially in the savanna in South Africa (Li et al., 2020c; Roques et al., 2001), northern Chihuahuan desert grasslands in southwestern North America (Caracciolo et al., 2016), and typical steppe in the Inner Mongolia grassland of China (Chen et al., 2015; Li et al., 2016a; Peng et al., 2013). Shrub encroachment negatively impacts the ecosystem processes of carbon cycle and resource redistribution and threatens local biodiversity, further affecting ecosystem structure, functioning and services (Li et al., 2016a; Zhou et al., 2019). Shrub aboveground biomass (AGB), as a key indicator of the carbon sink, plays a vital role in our attempts to understand the change of energy flow and material cycle in shrub-encroached grasslands. Thus, monitoring the spatial pattern of encroached shrub AGB, is essential for assessing the impact of shrub encroachment on grassland ecosystems, and hence provides a scientific basis for ecosystem restoration and sustainable grassland management. Traditional field sampling is often expensive and time-consuming and is challenging to collect shrub AGB non-destructively over large areas. To complement in-situ measurements, remotely sensed estimation of spatially continuous shrub AGB can fill in the gaps (Eisfelder et al., 2011; Lu, 2007).

In the Inner Mongolia Autonomous Region of China, over 5.1×10^4 km^2 grassland has been encroached by shrub species — *Caragana microphylla* (Peng et al., 2013; Zhang et al., 2006). Although *C. microphylla* is one of the tallest species on the steppe landscape, its height is generally lower than 2 m and the crown width is rarely exceeding 2 m. This renders coarse-resolution images (e.g. MODIS, HJ-1A/B, and Landsat OLI $\geq$ 30 m pixel) inadequate to describe the structural changes (e.g. biomass and density) (Xu et al., 2010; Zandler et al., 2015b; Zhou et al., 2013). In addition, coarse-resolution images usually focus on quantifying relative shrub cover per area (Jones et al., 2018), constraining applications that understand the effect of the structural change of encroached individual shrubs or shrub patches on ecological functions. In contrast, the distribution and biomass of individual shrubs could reflect the encroachment phase, but little attention has been paid to the mapping of individual shrubs. Therefore, high-resolution maps were required to characterize individual shrubs or patch dynamics in detail, which can be used to further calibrate and validate coarse maps (Li et al., 2020a).

As testified by existing studies, individual shrubs or shrub patches could be delineated using high-resolution satellite images or aerial photos by threshold or decision tree method (Goslee et al., 2003), object-based classification (Laliberte et al., 2004), wavelet analysis (Strand et al., 2006), and machine learning or deep learning (Gessner et al., 2013; Ludwig et al., 2016). Furthermore, the individual shrub AGB can be calculated from allometric equations using derived canopy areas or crown width (Adhikari et al., 2017). Nevertheless, even panchromatic satellite images with the highest resolution of 31 cm (WorldView-3 and WorldView-4) can still be difficult for the accurate recognition of dwarf *C. microphylla*. Unmanned aerial vehicle (UAV) has shown great potential in vegetation classification or species identification by acquiring centimeter level or higher resolution images without cloud limitation (Cao et al., 2018; Guo et al., 2021; Prosek and Simova, 2019). This provides a new pathway to identify small-sized shrubs, such as *C. microphylla*, and further supports the spatially continuous mapping of shrub AGB at individual scale (Guo et al., 2021). Moreover, UAV-based photogrammetric structure-from-motion (SfM) algorithms have been applied to detect canopy height or volume for biomass estimation by switching from ultrahigh-resolution images to point clouds (Cooper et al., 2017; Cunliffe et al., 2016; Li et al., 2016b; Zahawi et al., 2015). However, SfM processing may be insufficient for very dwarf vegetation, due to limitations with the vertical uncertainty of derived canopy height model (CHM) (Cunliffe et al., 2016; Zahawi et al., 2015).

Compared to the limited penetration capability of UAV-based digital photogrammetric techniques (Kalacska et al., 2017), laser pulses from Light Detection and Ranging (LiDAR) can penetrate the vegetation canopy and has shown great potential for capturing 3D structural characteristics of vegetation canopy (e.g. tree height, canopy or stand area, and canopy volume). Few studies, however, have attempted to estimate shrub AGB with LiDAR data in semiarid shrub-dominated systems (Nystrom et al., 2012; Streutker and Glenn, 2006; Vierling et al., 2012), although it has been widely applied in forest ecosystems (Bazezew et al., 2018; Sheridan et al., 2015; Wallace et al., 2017). The relatively low point density (e.g. < 4 points/m^2) and large laser footprint (e.g. > 5 m) of airborne LiDAR or spaceborne LiDAR (e.g. ICESat-2) are generally too coarse to accurately derive the canopy structure or volume of encroached shrub individuals with short (typically < 2 m) and open-branching canopy morphology (Coops et al., 2004; Li et al., 2020b; Vierling et al., 2012). A recent plot-stand example of mapping AGB of low-stature shrubs in Arctic tundra indicated that canopy volume derived from airborne LiDAR with high point cloud density (27 points/m^2) produced acceptable prediction accuracy (Greaves et al., 2016). The UAV-based LiDAR with low flight altitude allows for acquiring higher point density and smaller footprint size than airborne LiDAR, providing the possibility of capturing more canopy architecture details of individual shrubs. In addition, many studies demonstrated that the prediction accuracy of regional shrub AGB could be improved by combining the spectral properties and textural information derived from high-resolution optical imagery and structural properties extracted from LiDAR (Almeida et al., 2019; Ku and Popescu, 2019; Riegel et al., 2013).

Compared to airborne or UAV-LiDAR, Terrestrial Laser Scanning (TLS, also known as Terrestrial LiDAR) can obtain a much higher point cloud density, allowing for accurate estimation of canopy structural parameters of vegetation. TLS has been proved to be a powerful tool to predict the AGB without destructive sampling in arctic tundra and sagebrush ecosystems (Greaves et al., 2015; Olsoy et al., 2014; Wijesingha et al., 2018). Many volume-based approaches have been successfully applied in the AGB estimation of individual shrubs based on the TLS point clouds (Olsoy et al., 2014; Vierling et al., 2012). However, due to the spatial limitation of TLS, TLS-derived biomass has been used to validate the estimated biomass by airborne LiDAR as a ground reference value on the quadric scale (Greaves et al., 2017). Therefore, it is worth an in-depth exploration of whether TLS is capable of predicting the individual shrub AGB with high accuracy, leading to an integrated method of nondestructive AGB estimation of individual shrubs, such as *C. microphylla*, derived from UAV systems.

In this study, we aim to: 1) investigate if a combination of high resolution UAV-based multispectral image and LiDAR data can accurately separate individual shrubs in *C. microphylla* dominated semi-arid grasslands; 2) examine the capability of individual shrub AGB mapping using UAV-based multispectral imagery only, LiDAR only, and a combination of both sources, respectively; 3) determine the dominant shrub AGB indicators selected from geometric, spectral, textural, and volumetric features; and 4) explore the feasibility of TLS-derived individual AGB to validate the UAV-based AGB estimates without additional destructive harvesting.

2. Materials

2.1. Study area

The study was conducted in a typical shrub-encroached grassland, which is an experimental site of the Inner Mongolia Grassland Ecosystem Research Station of the Chinese Academy of Sciences (Fig. 1), located in the northeast of Xilinhot city, Inner Mongolia, China. The experimental platform covers an area of approximately 66 ha (44°22′08

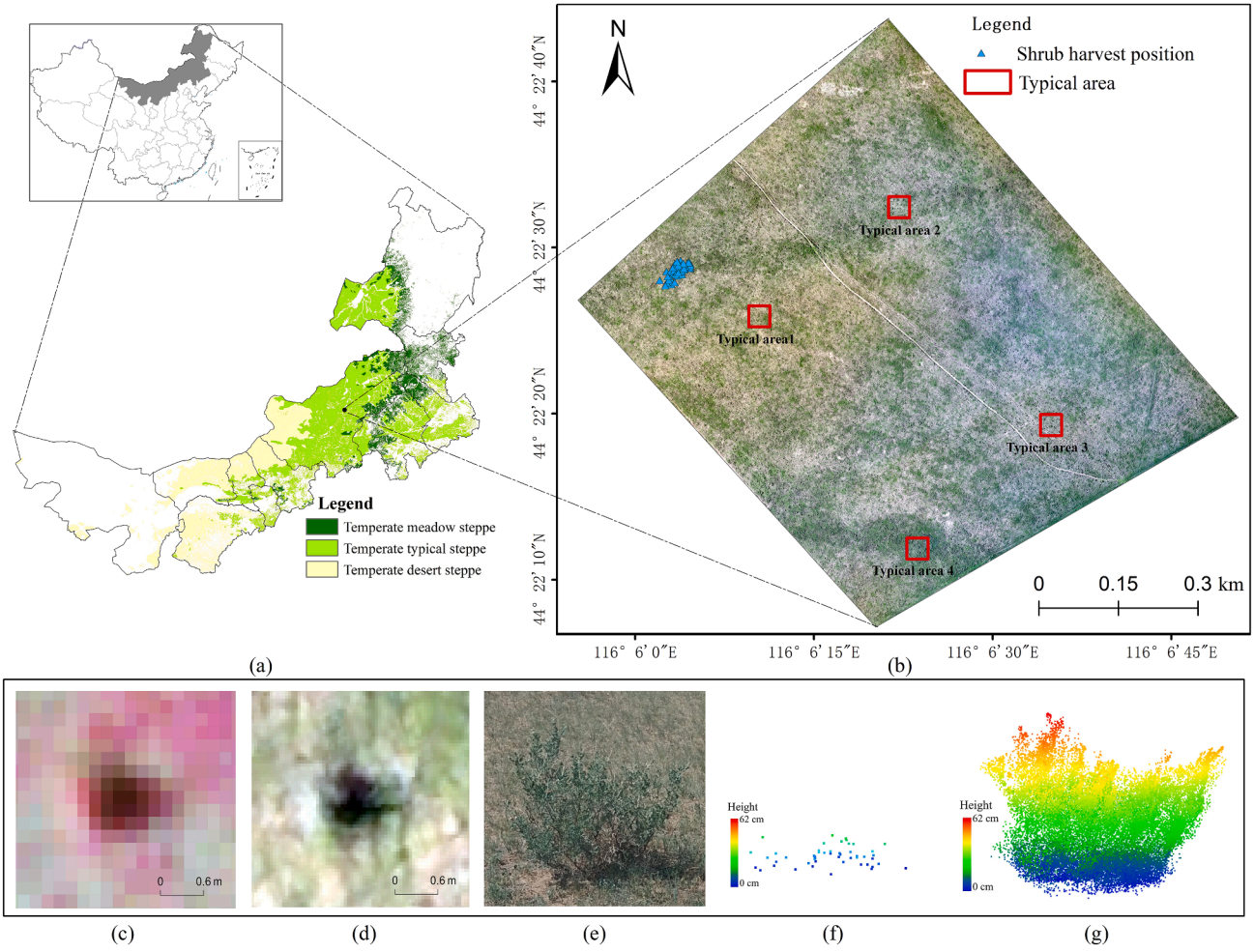

Fig. 1. Location of study area (a). Study area with UAV-based multispectral imagery shown in true color composition, the positions of individual shrubs in shrub harvest plots (blue triangles), and four typical areas (red boxes) for validation of individual shrub extraction (b). Display of a shrub in the study area with multispectral image (c), RGB image (d), digital photo (e), UAV-LiDAR point clouds (f), and TLS point clouds (g). (For interpretation of the references to color in this figure legend, the reader is referred to the web version of this article.)

"N-44°22′44″ N, 116°5′58″ E-116°6′50″E), with an altitude ranging from 939 m to 952 m. Due to the influence of a semiarid climate with continental monsoon characteristics, the study area is cold and dry in winter, and warm and humid in summer with the mean annual temperature of 3.8 °C and mean annual precipitation of 269.5 mm (1980–2019). The growing season typically lasts about 150 days from April to September. The land cover types across the study area are composed of grass, shrub, and sandy soil. *C. microphylla* is the only shrub species and irregularly distributed in the study area mainly by individual plants (Fig. 1e), with a mean height of 0.27 m and crown area of 97 cm × 66 cm. With a developed root system, *C. microphylla* can better tolerate the arid conditions compared to the two dominant grass species, *Leymus chinensis* and *Stipa krylovii*.

2.2. Data collection

2.2.1. UAV-based multispectral imagery

The multispectral imagery was acquired over the study area using the Parrot SEQUOIA multispectral sensor in July 2017. Equipped with a multispectral camera comprising of four bands in the red (660 nm), green (550 nm), red edge (735 nm), and near infrared (790 nm) and an RGB camera, the SEQUQIA sensor can capture both visible and infrared imagery during a flight. We mounted the SEQUOIA sensor on a fixed-wing unmanned aerial vehicle (UAV), called EY130 drone designed by Beihang University. The UAV flew over 80 m above the ground with a side and front overlap rate of both 80%, yielding a spatial resolution of 16 cm for the multispectral imagery and 4 cm for the RGB imagery, respectively. All required multispectral and RGB images were automatically mosaicked into the entire imagery across the study site using Agisoft PhotoScan (Agisoft, St. Petersburg, Russia), respectively. The mosaic imagery was then geometrically corrected based on collected ground control points. The normalized difference vegetation index (NDVI) was derived from the final corrected multispectral imagery.

2.2.2. UAV-based LiDAR data

The LiDAR point cloud data were acquired immediately after the multispectral imagery using the mini-UAV LiDAR system-AOEagle developed by the Academy of Opto-electronics, the Chinese Academy of Sciences (Teng et al., 2017). The scanner was flown 16 m above the ground with a detection angular resolution of 0.125° and trajectory width of 30 m, leading to a footprint size of 3.5 cm and an average point cloud density of 99.56 points/m^2. The point cloud data were first filtered to remove noisy data and classified into vegetation and ground points using the commercial software Terrasolid (Terrasolid, Helsinki, Finland). The raster image of the Digital Elevation Model (DEM) was then generated from the classified ground points. The LiDAR point clouds were also height-normalized by calculating the differences between the first laser returns (i.e., actual elevation) and DEM. The canopy height model (CHM) was derived by interpolating the height-normalized vegetation points using the LAStools software (Rapidlasso GmbH,

Gilching, Germany) at the same pixel resolution as the multispectral imagery. The DEM, CHM and multispectral imagery were finally co-registered with a root mean squared error (RMSE) within 8 cm using the registration tool from ENVI 5.3. The coordinate reference systems of all data sources in the study were registered to the Universal Transverse Mercator (UTM) Zone 50 N/WGS −84 projection coordinate system. In addition, the potential water stream networks were extracted from the DEM data by the hydrological analysis in ArcMap 10.2 (Esri. Inc., Redlands, CA, USA), which were used as ancillary data to describe the spatial distribution pattern of individual shrub AGB.

2.2.3. Field measurements and TLS data

The field measurements were immediately performed after the UAV campaigns. A representative area in this study was selected to set up two shrub harvest sample plots of 20 m × 20 m during the growing season in August 2017 (Fig. 1b). The geographical corner coordinates of each sample plot and shrub harvest position were measured with the Trimble Pro 6H GPS system (Trimble Inc., Sunnyvale, CA, USA) running in a post-processed kinematic (PPK) mode with an accuracy of approximately 10 cm. For each plot, the TLS point cloud data were scanned using a FARO Focus S70 terrestrial laser scanner (FARO Technologies Inc., Lake Mary, FL, USA). Five different scanning positions were placed in the center and opposing sides of each sample plot to minimize occlusion. Four target reflector poles with a height of 1.2 m were placed at each corner of the sample plot to improve the registration accuracy of different scanning positions before scanning. All the scans were completed on windless days to reduce shrub movement. After scanning, the height of each shrub in each plot was measured. However, it is still difficult for shrubs below 10 cm to distinguish from similar grasses based on our UAV-based imagery and LiDAR data. All shrubs higher than 10 cm (n = 48) were destructively harvested by clipping the shrubs to the ground surface. All harvested shrub samples were oven dried at 65 °C for at least 48 h and then weighed to obtain AGB (g) for each individual shrub.

The TLS data preprocessing was performed using the FARO SCENE software and LAStools software, including registration, noisy point removal, filtering, and height normalization. First, five scans of each sample plot were co-registered and merged interactively based on the four target reflector poles in FARO SCENE software, resulting in an average point density of 75,924 points/m^2. Second, the registered point

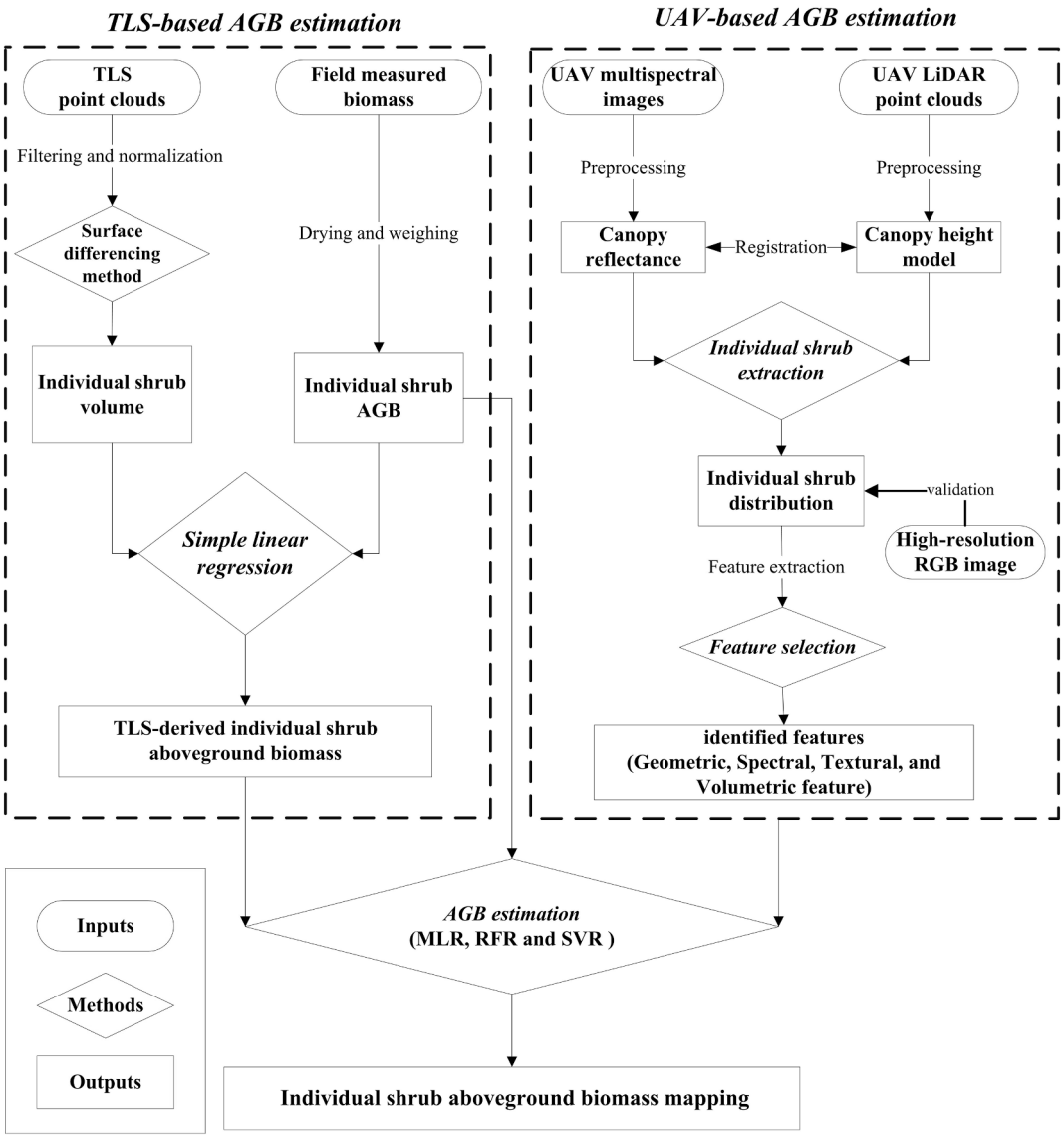

Fig. 2. Flow chart of the main processing steps for predicting individual shrub aboveground biomass with the combination of TLS data, UAV multispectral imagery, and LiDAR data in the study area.

clouds were denoised and filtered using the LAStools software, and then classified as vegetation and ground points. The height of the point cloud was normalized to obtain the actual height of shrub individuals. Finally, the filtered point clouds were manually segmented to isolate individual shrub for subsequent AGB estimation using the CloudCompare software (EDF Lab Paris-Saclay, Palaiseau, French).

3. Methods

3.1. Overview of methodology

Both UAV-based and TLS-based individual shrub AGB estimation were used in this study (Fig. 2). For the UAV-based individual shrub AGB estimation, the individual shrubs were firstly delineated from the grasses and sandy soil based on their distinguishable thresholds in NDVI and CHM. Then, the geometric, spectral, and textural, and volumetric features of extracted individual shrubs were selected and derived from the multispectral imagery and LiDAR data as predictors of shrub AGB. Regression modeling methods, including multiple linear regression (MLR), random forest regression (RFR), and support vector regression (SVR), were applied to determine the optimal estimation model of individual shrub AGB. The optimal estimation model was used to map the spatial pattern of individual shrub AGB. For the TLS-based AGB estimation of individual shrubs, an optimal volume-based AGB estimation model for *C. microphylla* was applied by comparing three volumetric methods, including global convex hull, voxel, and surface differencing. The TLS-derived AGB of individual shrubs was evaluated by field-measured AGB to determine whether it can be scaled up to a larger area as a true value to validate the UAV-based AGB estimation of individual shrubs without additional destructive harvesting.

3.2. Extraction of individual shrubs based on UAV data

Considering the spectral and height variations of shrubs, grasses and sandy soil, we used a threshold method to separate individual shrubs from grasses and sandy soil by combining the NDVI and CHM data. First, 100 manually digitized polygons of grass, shrub, and sandy soil were randomly selected from the high-resolution RGB imagery (4 cm) as training samples to represent their variations in spectra and height over the study area, respectively. Second, we derived the NDVI and canopy height for each sample. We also calculated the mean metric value (Mean $= \sum_{i,j=0}^{N-1} iP_{i,j}$, $P_{i,j}$ is the co-occurrence matrix) of gray level co-occurrence matrix (GLCM) of rasterized CHM by setting 3×3 window size and 16-bit grayscale quantization for these samples, which indirectly reflects the variation in height, rather than the actual height. Finally, One-way ANOVA analysis with Tukey (multiple-comparison) tests was performed to determine the thresholds by examining the statistical differences of NDVI, canopy height, and GLCM mean value of CHM among the three types of samples. The decision tree method was then used to classify sandy soil, shrub, and grass based on the selected thresholds. The identified individual shrub pixels were finally aggregated into an individual shrub polygon based on RasterToPolygon toolbox in ArcGIS Desktop 10.2 (Esri. Inc., Redlands, CA, USA). The extracted individual shrub polygons could be visually validated compared to their positions and area in the high-resolution RGB image (4 cm). Four typical areas were randomly selected to evaluate the extracted individual shrubs (match, omission and commission).

3.3. Feature selection from UAV data

To test the modeling ability of spectral, geometric, textural and volumetric features for individual shrub AGB, we extracted a total of 111 feature variables from UAV multispectral imagery and LiDAR data, including 5 geometric features, 30 spectral features, 48 textural features, and 28 volumetric features (Table S1 in Supplementary Materials).

The geometric, spectral, and textural features for each extracted individual shrub polygon were derived from the UAV multispectral imagery. Geometric features can reflect the growth morphology and development status of shrub individuals, including the canopy area, perimeter, thickness, length of the major axis, and length of the minor axis. Spectral features indirectly capture the canopy cover and have been successfully applied to estimate vegetation biomass (Berner et al., 2018; Chen et al., 2018; Zandler et al., 2015a). Five vegetation indices, including NDVI, ratio vegetation index (RVI), wide dynamic range vegetation index (WDRVI), soil-adjusted vegetation index (SAVI), and difference vegetation index (DVI), were selected to calculate their statistical data (maximum, minimum, mean, standard deviation, range and sum) of each shrub as the spectral features of shrub AGB estimation. Textural features can effectively remedy the effect of the spectral saturation problem of vegetation indices for the biomass prediction. Eight textural metrics of GLCM (Haralick et al., 1973), including mean, variance, homogeneity, contrast, dissimilarity, entropy, second moment and correlation, were calculated, and then their statistics value (maximum, minimum, mean, standard deviation, range and sum) of each extracted individual shrub polygon were used as the predictors of shrub AGB. The GLCM was calculated based on the first principal components PC1 (variance contribution: 98.14%) of the principal component analysis (PCA) performed on the UAV multispectral image using the ENVI 5.3 software, and the parameters were set as follows: the processing window size was 3×3, the grayscale quantization was 16, and the co-occurrence shift in the X and Y direction was 1 ([0, 1], [1, 1], [1, 0], and [1, –1]).

The volumetric features mainly include the statistical variables for the height and volume derived from UAV-LiDAR point clouds for each individual shrub. The volume of individual shrubs was also calculated using the surface differencing method with the optimal volume value determined empirically by testing different point cloud height variables and grid size parameters (Greaves et al., 2015). The statistical variables related to height distribution, including percentiles, skewness, kurtosis, and coefficient of variation, were calculated using the FUSION LDV 3.8.0 open source software.

To reduce the redundancy of variables and optimize the performance of the UAV-based AGB estimation models, the forward stepwise regression method based on the Akaike Information Criterion (AIC) minimization was used (Yamashita et al., 2007) to select the optimal predictors from volumetric features (LiDAR only), geometry + textural + spectral features (multispectral imagery only), and volumetric + geometric + textural + spectral features (multispectral imagery + LiDAR), respectively. For multispectral imagery only, the optimal spectral, geometric and textural predictors were also selected alone from spectral features, geometric features, and textural features, respectively. Only feature variables with variance inflation factor (VIF) less than 5 were retained to eliminate the multicollinearity effects. Then, a random forest regression algorithm (scikit-learn 0.22, python) was performed to further determine variable importance of the optimal predictors for individual shrub AGB estimation based on the Gini importance. The Gini importance was calculated by randomly ranking the predicted variables with out of bag (OOB) data in terms of the total reduction of node impurities (Strobl et al., 2008).

3.4. UAV-based AGB estimation models and validation

Three regression methods, including multiple linear regression (MLR), random forest regression (RFR) (Breiman, 2001), and support vector regression (SVR) (Suykens and Vandewalle, 1999), were applied for the AGB estimation of individual shrubs. To test the potential of mapping individual shrub AGB using different UAV-based data sources (multispectral images only, LiDAR only, and their combination), the shrub AGB estimation models were constructed based on: 1) the selected spectral, geometric, and textural features derived from multispectral imagery; 2) the selected volumetric features derived from the LiDAR point cloud; and 3) all selected feature variables. All selected feature

variables were first standardized based on the Min-Max normalization method as independent variables to avoid weight saturation. The three regression methods were carried out using scikit-learn's 'LinearRegression', 'RandomForestRegressor' and 'SVR' modules. MLR is a regression analysis method to explore the relationship between multiple independent variables and dependent variables. To satisfy the statistical hypotheses of multiple linear regression, the AGB measurements were transformed by natural logarithm as dependent variables. Unlike the MLR methods, both SVR and RFR belong to the machine learning methods described as non-parametric and generally are not concerned with the error distribution. However, their model performances are mainly constrained by model parameters. Therefore, the grid search function 'GridSearchCV' provided by scikit-learn was used to determine the optimal model input parameters of SVR and RFR, respectively (Table S2). The coefficient of determination (R^2) and root mean squared error (RMSE) were calculated to quantify the model performance of all the constructed models based on the leave-one-out cross-validation (LOOCV) (Brovelli et al., 2008). Namely, the UAV-based AGB estimation models were trained n times (n = 48) with n-1 samples used in training and the remaining one sample used for testing. The optimal regression model was determined by the lowest cross-validation error compared with the field measured AGB ('harvest-calibrated model').

The consistent mean and range of spectral, geometric, volume, and texture metrics of shrubs in the field samples and the four typical areas (*t*-test, Fig. S1 in Supplementary Materials) proved the AGB model training data were representative of those in the entire study area. Therefore, we finally used the optimal biomass estimation model to map the AGB of individual *C. microphylla* over the entire study area. In addition, a paired *t*-test was applied to evaluate the significance of differences between predictive models based on multispectral imagery only, LiDAR only, and their combination, respectively.

3.5. TLS-based individual shrub AGB estimation

Given that the performance of recent volumetric approaches depends to some extent on the point cloud density and specific-species structural characteristics, there is no universally best method for the biomass estimation of *C. microphylla*. We compared the ability of three volumetric approaches for estimating shrub AGB, including the global convex hull method (Olsoy et al., 2014), voxel method (Olsoy et al., 2014), and surface differencing method (Greaves et al., 2015). Among these methods, surface differencing method showed the best performance, followed by the voxel method, and the global convex hull method showed the weakest relationship with field measured biomass (Table S3).

We limited our analysis to the surface differencing method as our optimal method for estimating shrub AGB. The point clouds were divided into square grids on the XY plane, and then the height parameters of point clouds within each grid were calculated. The shrub volume was finally estimated as the product of the height parameters and the grid area in each grid. A simple linear regression (SLR) model was used to evaluate the relationships between the harvested individual shrub AGB and the volume derived from TLS point clouds. The optimal grid size for each surface was empirically determined by varying the grid size between 1 cm and 15 cm in steps of 1 cm, and the optimal height parameters were selected from maximum height (MAX), 95th percentile height (P95), standard deviation of height (Std), and mean height (Mean) by comparing the change in R^2 and RMSE utilizing LOOCV.

4. Results

4.1. Extraction of individual shrubs

Statistical differences were detected in NDVI, canopy height, and GLCM mean value of CHM between grass, shrub, and sandy soil (Fig. 3). We first selected the maximum NDVI value of sandy soil (NDVI = 0.52)

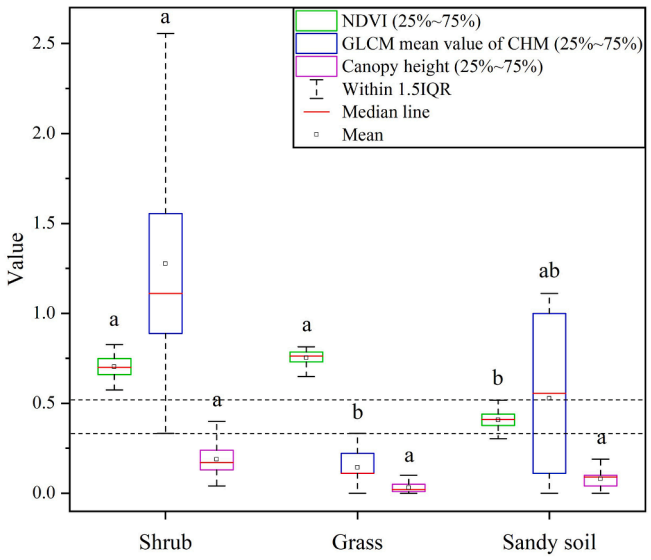

Fig. 3. Boxplots and statistical differences of NDVI, canopy height and GLCM mean value of CHM between samples of shrub, grass, and sandy soil. Lowercase letters above bars indicate statistical differences in variables between sample types using ANOVA with Tukey multiple-comparison tests ($P < 0.05$). The differences with any same letter are not significant. IQR denotes interquartile range. (25–75%) of NDVI, GLCM, and CHM demotes their value interval from 25% to 75%, respectively.

as the threshold to distinguish vegetation (shrub and grass) and sandy soil (Fig. 3), based on the significant statistical differences in NDVI in shrub and grass ($P < 0.05$). Furthermore, the fact that shrubs were statistically higher than grass in GLCM mean value of CHM (Fig. 3), promoted the selection of the maximum GLCM mean value of grass (mean GLCM = 0.33), rather than the canopy height as the threshold to extract the individual shrubs from the grass. Results of individual shrub extraction were visually validated in the high-resolution RGB image (Fig. 4a). Specifically, 356 out of the 388 reference shrubs were correctly matched (91.8%) across the four typical areas (Fig. 4b). The omission error (8.2%) was mainly caused by small shrubs difficultly detected because of the limitation of spatial resolution (6.2%), and under-segmentation caused by large shrub patches/stands with overlapping crowns (2.0%). Only 12 extra shrubs were incorrectly extracted due to the presence of over-segmented large sparse-canopy shrubs, corresponding to a commission error of 3.1% across the four typical areas.

4.2. Feature selection from UAV data

The final selected results of the feature variable sets are shown in Table 1. For the volumetric features extracted by UAV-LiDAR data, the volume calculated with the standard deviation of the 50th percentile height was selected, further verifying that the volume was an important indicator of the individual shrub AGB. Because of the multicollinearity effects of all selected feature variables derived from multispectral imagery, only the Thickness, Contrast_SUM, and RVI_MAX corresponding to geometric, textural, and spectral features were selected as the predictors, instead of all the combination of 8 feature variables selected alone from geometric, textural, and spectral features. For the multispectral imagery + LiDAR, the selected variables were almost consistent with the combined results of the above two selections. However, the shrub volume was not selected due to its strong autocorrelation with other selected feature variables (Pearson correlation coefficient is 0.89 for Contrast_SUM, 0.83 for THICKNESS, and 0.55 for RVI_MAX).

The Gini importance ranking of ten selected feature variables (Volume, H_P50, DVI_RANGE, RVI_SUM, Thickness, Major axis, Contrast_SUM, Mean_RANGE, Variance_STD, RVI_MAX) is shown in Fig. 5.

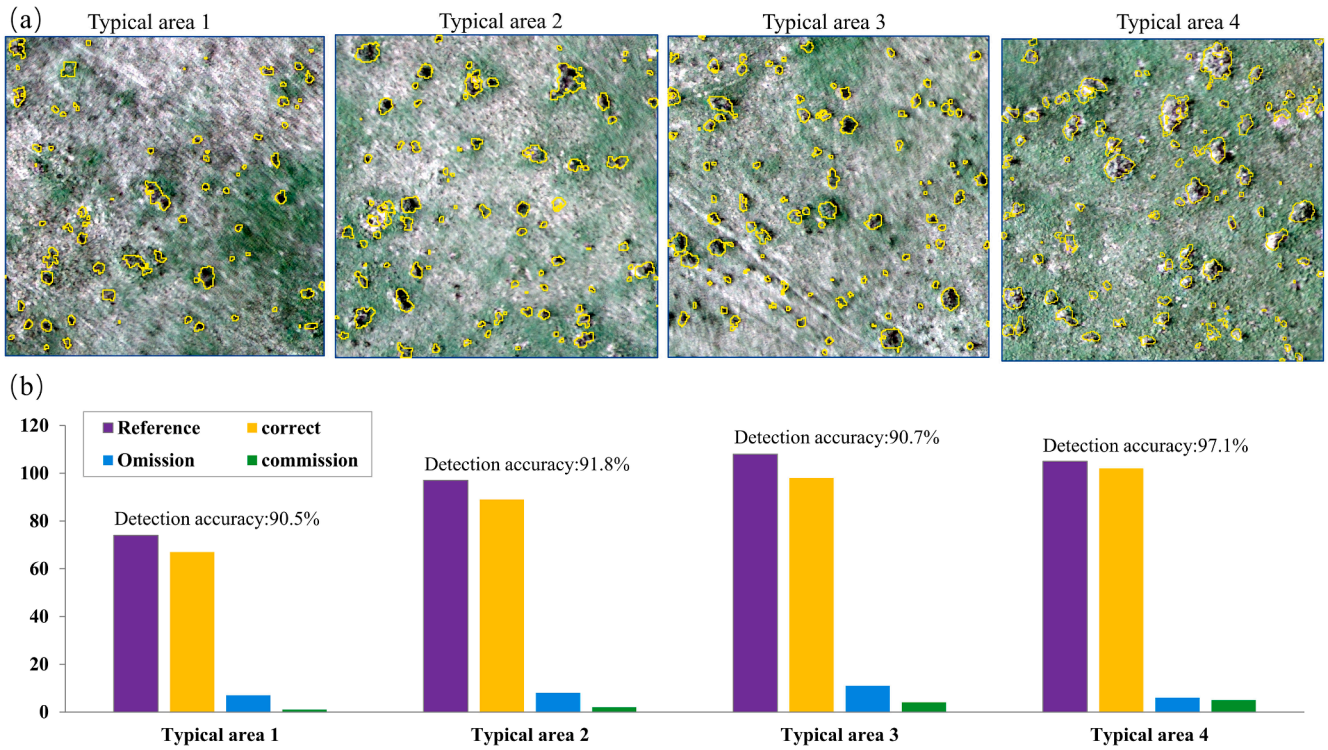

Fig. 4. Results of individual shrub extraction in the RGB imagery with 4 cm spatial resolution (a), and the number of reference shrubs, correctly matched shrubs, missed shrubs (omission), and extra individual shrubs (commission) in four typical areas (b).

Contrast_SUM, Volume, Thickness, and RVI_SUM was the optimal indicator of textural feature, volumetric feature, geometric feature, and spectral feature, respectively. Contrast_SUM was the strongest predictor of individual shrub AGB out of the ten selected variables. Surprisingly, the individual shrub volume ranked second in the prediction of shrub AGB, followed by geometric feature, Thickness, which represents the crown size of individual shrubs. In contrast, the optimal spectral predictor, RVI_SUM, had a relatively weak ability to estimate individual shrub AGB among all the four features, i.e. textural feature > volumetric feature > geometric feature > spectral feature (Fig. 5).

4.3. Individual shrub AGB prediction and validation

The SVR method showed the highest estimation accuracy based on LiDAR data alone and multispectral imagery data alone (Table 2). For the combined LiDAR and multispectral imagery data, the MLR method had the best performance. However, the prediction accuracy of SVR and MLR was almost indistinguishable for all three cases. By contrast, the RFR method had a relatively large RMSE among the three models (Table 2). The SVR method was selected as the best estimation model for the LiDAR data and multispectral imagery, respectively, and the MLR method was selected as the best estimation model for the combined data sources (LiDAR + multispectral imagery) (Fig. 6).

The model results indicated that the high-resolution multispectral imagery performed better in individual shrub AGB estimation than LiDAR (Fig. 6). Although the estimation model combined the multispectral imagery and LiDAR data performed best, the prediction accuracy was just slightly improved compared to the multispectral imagery only. The paired *t*-test also indicated that there are no significant differences between all these models.

The MLR model was finally applied to map the individual shrub AGB based on the combined multispectral imagery and LiDAR point clouds (Fig. 7). The individual shrub AGB in the study area was mainly distributed between 200 and 400 g. Visually, the dense distribution and high AGB of individual shrubs were mainly distributed around the potential water streams (Fig. 7).

4.4. TLS-based individual shrub AGB estimation

As expected, the results of LOOCV showed that TLS-derived volume was a more reliable indicator of shrub AGB for individual *C. microphylla* ($R^2_{LOOCV} = 0.91$, RMSE = 78.98 g) (Fig. 8b) than UAV-based individual shrub AGB estimation. The optimal volume was achieved with a grid size of 7 cm and a standard deviation of height of point clouds within each grid based on the surface differencing method (Fig. 8a). The model accuracy initially increased and then decreased with increasing grid size, reaching the highest accuracy at 7 cm (Fig. 8a). Compared to the standard deviation, the remaining height parameters (maximum height, 95th percentile height, and mean height) showed relatively weak results (R^2_{LOOCV} = 0.82–0.87, RMSE = 83.14–126.65 g) in our experiment (Table S3).

5. Discussion

5.1. Individual shrub extraction

Accurately isolating an individual shrub is a prerequisite for estimating individual shrub AGB. Our comparisons with field observations indicate that the combination of UAV multispectral and LiDAR data allows individual shrub detection with good accuracy. The accuracy of individual shrub identification may be influenced by the shrub morphological characteristics, identification algorithms, point cloud density and footprint size of LiDAR, and the resolution of the optical imagery.

Within our study area, the actual height of most shrubs detected by LiDAR is higher than grasses and ground surface. However, some UAV-LiDAR returns of grasses or small shrubs may be erroneously classified to ground returns, resulting in the generated DEM higher than actual ground surface (Riaño et al., 2007; Vierling et al., 2012). Moreover, the small wind-eroded dunes may also be misclassified as shrubs. These two

Table 1
Feature variables selection for individual biomass estimation based on forward stepwise regression with the variance inflation factor (VIF) < 5.

Variable group	Variables selected	Description	VIF	AICc
Volumetric features (LiDAR only)	Volume	Volume calculated using the surface difference method with standard deviation of height parameter:H_P50.	1.38	61.30
	H_P50	50st percentile value of height	1.38	57.51
Spectral features	DVI_RANGE	Range of Difference Vegetation Index (DVI): NIR-R for an individual shrub.	1.99	76.83
	RVI_SUM	Sum of Ratio vegetation index: NIR/R for an individual shrub	1.99	60.91
Geometric features	Thickness	Distance between the deepest point and the pixels around it in a shrub region.	2.68	60.22
	Major axis	Length of the long axis of the individual shrub.	2.68	53.16
Textural features	Contrast_SUM	Sum of textural feature: Contrast for an individual shrub.	2.30	65.24
	Mean_RANGE	Range of textural feature: Mean for an individual shrub.	3.80	54.98
	Variance_STD	Standard deviation of textural feature: Variance for an individual shrub.	2.13	49.51
Geometry + Textural + Spectral features (multispectral imagery only)	Thickness	Distance between the deepest point in a shrub region and the pixels around it.	2.53	60.22
	Contrast_SUM	Sum of textural feature: Contrast for an individual shrub.	2.87	46.02
	RVI_MAX	Maximum of Ratio vegetation index: NIR/R for an individual shrub.	1.48	41.84
Volumetric + Geometric + Textural + Spectral features (multispectral imagery + LiDAR)	Thickness	Distance between the deepest point in a shrub region and the pixels around it.	2.77	60.22
	Contrast_SUM	Sum of textural feature: Contrast for an individual shrub.	2.87	46.02
	RVI_MAX	Maximum of Ratio vegetation index: NIR/R for an individual shrub.	1.54	41.84
	H_P50	50th percentile value of height.	1.46	39.90

classification errors of vegetation and ground returns can lead to the underestimation of vegetation height and individual shrubs, limiting the capability of canopy height to effectively detect the individual shrubs. The spectral vegetation indices have the promise for reducing these errors (Riaño et al., 2007). Considering the relatively simple mosaic landscape of shrubs, grasses and sandy soil, we used a threshold method of combined NDVI and CHM to separate individual shrubs from grasses and sandy soil. Besides, in contrast to the elliptical or conical crown shapes for coniferous or broad-leaved forest species, the crown shape of the *C. microphylla* tends to be flat. The inherent vertical error of UAV-based LiDAR increases the difficulty in directly using the methods of

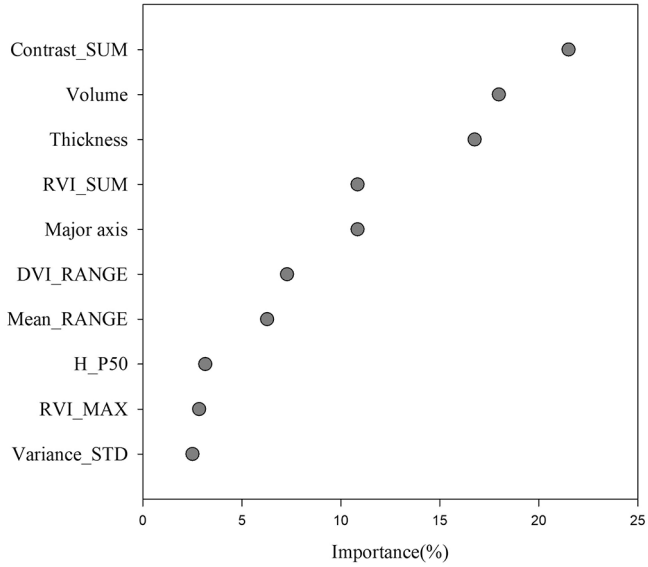

Fig. 5. Gini importance ranking of all selected feature variables.

Table 2
Accuracy comparison of the shrub AGB prediction models established by different regression methods and different feature variables.

Method/Feature source	LiDAR	Multispectral imagery	LiDAR + Multispectral imagery
	R^2_{LOOCV} /RMSE (g)	R^2_{LOOCV} /RMSE (g)	R^2_{LOOCV} /RMSE (g)
MLR	0.76^{***}/ 128.72	0.83^{***}/106.65	0.86^{***}/101.97
RFR	0.78^{***}/ 147.62	0.83^{***}/124.88	0.84^{***}/123.03
SVR	0.77^{***}/ 123.33	0.83^{***}/106.46	0.86^{***}/102.70

individual tree segmentation (e.g. local maxima algorithm or watershed algorithm) to separate short individual shrubs (Chang et al., 2013; Zhao et al., 2013). The ultrahigh-density point cloud data (e.g. >1000 points/m^2) and full-waveform LiDAR systems are expected to capture more 3-D canopy structural information of low-stature shrubs and detect shrub encroachment effectively (Madsen et al., 2020; Vierling et al., 2012).

Compared to LiDAR, the high-resolution optical imagery allows for identifying individual shrubs or shrub patches by involving spectral, textural, and geometric factors of different objects based on the object-based classification or threshold method (Goslee et al., 2003; Laliberte et al., 2004). Our previous study in this area also indicated the overall classification accuracy of shrub, grass, and sandy soil arrived 92% based on the object-based Bayes classification method only using the UAV-based optical images (Zhang et al., 2019), which was almost same as the threshold method in this study. It is also noteworthy that the spatial resolution of the multispectral imagery limits the extraction of individual shrubs smaller than its pixel size. Moreover, limited by flight altitude and camera quality, the error of shrub height derived from the SFM algorithm exceeded 30 cm based on our initial experimental test. As the UAV-based camera resolution further improved (e.g. <1 cm), it would be feasible to successfully detect small-size individual shrubs, and capture the shrub height variability using SfM or Multi-View Stereo (MVS)-based photogrammetry approaches, which have been proved to acquire grassland height with a mean absolute error of between 3.7 and 4.2 cm (Forsmoo et al., 2018). Furthermore, the classification accuracy of individual shrubs would also be improved with the fusion of spectral and vertical information derived from a single optical sensor (Prosek and Simova, 2019). In the future, we will further test this method with the

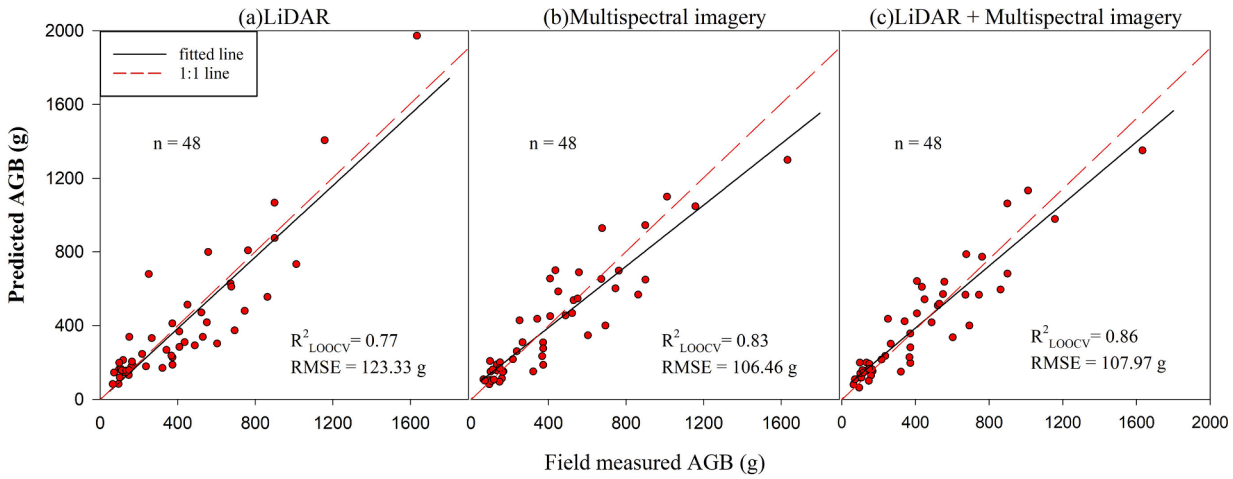

Fig. 6. Optimal individual shrub aboveground biomass (AGB) estimation based on LiDAR point clouds only using support vector regression (SVR) method (a), multispectral imagery only based on SVR method (b), and the combination of LiDAR point clouds and multispectral imagery using multiple linear regression (MLR) method (c).

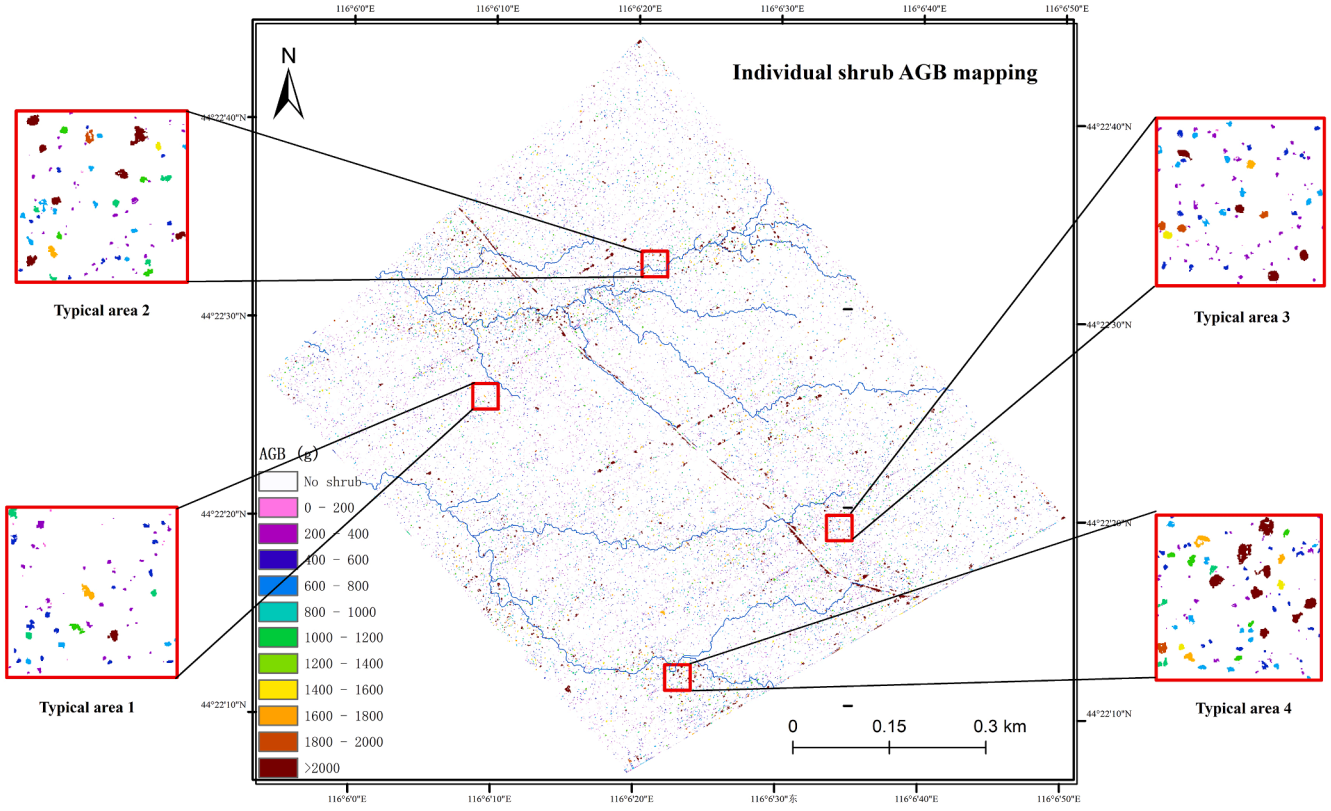

Fig. 7. Spatial pattern of individual shrub aboveground biomass (AGB) in the study area. Blue lines denote the potential water stream networks extracted from DEM. (For interpretation of the references to color in this figure legend, the reader is referred to the web version of this article.)

new ultrahigh-resolution optical imagery. Nonetheless, the resulting high time cost should also be considered, and a trade-off between the cost of flight efficiency and prediction accuracy needs to be investigated.

5.2. *Estimating individual biomass of C. microphylla*

Among the spectral, geometric, textural and volumetric features extracted from multispectral imagery or point cloud data, there is no consistent conclusion on which feature can obtain the best result for shrub biomass estimation (Adhikari et al., 2017; Berner et al., 2018; Sarker and Nichol, 2011). Previous studies mainly focused on the fusion of multi-source data, fully mining various information to improve the accuracy of biomass estimation. On one hand, the geometric features extracted from the two-dimensional multispectral imagery directly reflect the shrub size, but cannot mirror the changes of shrub vertical structure. On the other hand, although the spectral variation caused by shrub canopy density or health could indicate the changes of shrub biomass, the spectral change maybe no longer sensitive to high AGB because of spectral saturation problem. Textural features can minimize the saturation problem and have a good response to the change of shrub canopy structure in each growth period. Furthermore, the vertical structure parameters or volume closely related to AGB can be derived

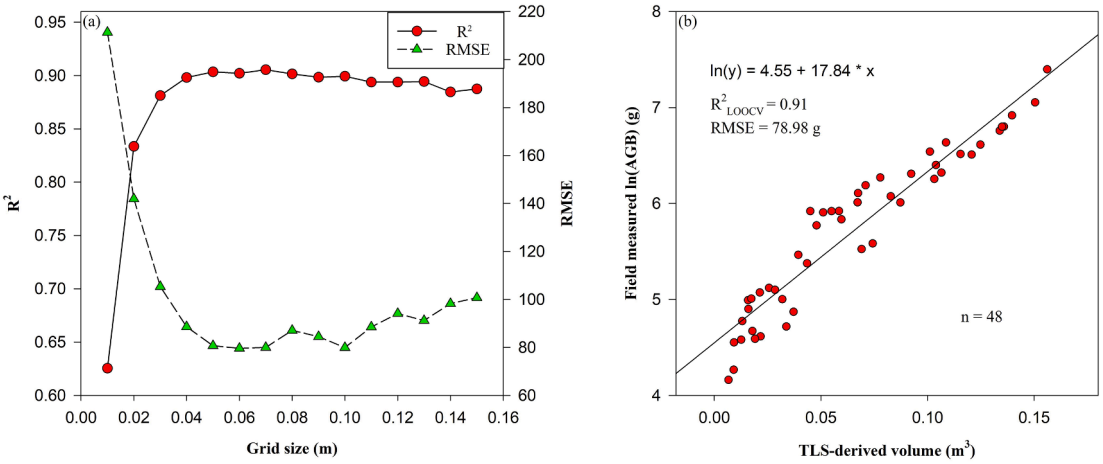

Fig. 8. Response of TLS-based shrub aboveground biomass (ln (AGB)) estimation R^2 to different grid sizes based on the surface differencing method (a). Optimal linear regression relationships between ln (AGB) and TLS-derived volume using surface differencing method ($p < 0.001$) (b).

from LiDAR-based point cloud data. The combination of all the four features can incorporate the horizontal and vertical structural information, and would be expected to improve the estimation accuracy. Therefore, in this paper we constructed and compared prediction models from the four aspects of geometry, spectrum, texture and volume to obtain the optimal estimation accuracy of individual shrub biomass.

The reported Gini importance ranking suggests that the textural variable-Contrast_Sum was the most important predictor of individual shrub AGB, whereas the spectral features showed relatively weak performance in predicting individual shrub AGB among all the four features. Consistent with many previous studies (Kelsey and Neff, 2014; Meng et al., 2016; Nichol and Sarker, 2011), texture processing demonstrated greater potential in predicting individual shrub AGB than spectral information ($R^2_{LOOCV} = 0.81$, RMSE = 116.23 g; Fig. S2 in Supplement Material), especially for multispectral imagery with high spatial resolution since finer structural or textural details within individual shrubs can be detected. With the UAV-based ultra-fine multispectral imagery, Constrast_sum represents the sum of spectral variability caused by the change of local leaf or stem density in different neighboring pixels within an individual shrub, further indicating total AGB of the individual shrub.

It is also noteworthy that the volumetric variable was only the second-best predictor of shrub AGB ($R^2_{LOOCV} = 0.76$, RMSE = 128.72 g; Fig. S2), largely owing to the underestimation of UAV-LiDAR derived canopy volume. Consequently, in our study, the inclusion of UAV LiDAR-derived volume did not improve the shrub AGB prediction. Moreover, the ability of different data sources for shrub AGB prediction indicate that UAV LiDAR might not have much advantage over the high-resolution multispectral image, especially for short shrubs with relatively sparse canopy structure. A previous study also found that the high-resolution optical imagery outperformed the discrete-return LiDAR in estimating AGB in a coastal plain wetland with young and small trees (Riegel et al., 2013). Besides, as discussed above, canopy height model can be achieved by converting UAV ultrahigh-resolution imagery to point clouds based on the SfM or MVS method at a much lower cost than LiDAR. Furthermore, a vegetation index weighted canopy volume model may benefit the biomass estimation from UAV-based ultra-high resolution images (Maimaitijiang et al., 2019).

The geometric canopy shape of individual shrubs, which is often unconsidered in the plot-level biomass estimation, also provides more effective information than spectral reflectance. It is widely held that the high-resolution multispectral image has been used to delineate and estimate the individual shrub canopy area or canopy width, further calculating biomass from allometric equations (Adhikari et al., 2017; Guo et al., 2021). The high explanatory power of canopy horizontal morphology ($R^2_{LOOCV} = 0.74$, RMSE = 137.44 g; Fig. S2) to shrub AGB also makes up for the error caused by the inaccuracy of height extraction to some extent.

The spectral features have the weakest performance for individual shrub AGB estimation ($R^2_{LOOCV} = 0.71$, RMSE = 139.99 g; Fig. S2) mainly because of the saturation problem for high AGB. Remarkably, the hyperspectral sensor, particularly with the short-wave infrared spectral region, holds promise for improving the spectral prediction of dwarf shrub AGB in this study area (Zandler et al., 2015a). Furthermore, many functional traits, such as the leaf content of chlorophyll, leaf mass per area, water and nitrogen, have been successfully retrieved from the multi- or hyperspectral data (Asner and Martin, 2009; Jetz et al., 2016; Zhao et al., 2016). This will advance our understanding of the ecological linkage between functional traits and ecosystem productivity caused by shrub encroachment. Therefore, with the textural, geometric and spectral advantage, the high-resolution multispectral image may be more suitable and cost-effective for estimating individual AGB of *C. microphylla* than UAV-based LiDAR.

5.3. Nondestructive individual shrub AGB mapping with TLS-based calibration

Our study further validated the potential of the TLS technique for individual shrub AGB estimation in a precise, cost-efficient and nondestructive way. By incorporating both vertical and horizontal architecture of individual canopies, TLS-derived canopy volume enables a vigorous proxy for individual shrub AGB. Previous studies indicated that the large and dense canopy volume calculated using the voxel-based method might be underestimated because the laser failed to fully penetrate into the interior of vegetation canopy, while the sparse canopy volume calculated using the global convex hull method might be overestimated due to the canopy gaps improperly entangled into the volume (Greaves et al., 2015; Olsoy et al., 2014). Through empirically optimizing different grid sizes and height variables, the surface differencing method overcomes the limitations of the above two methods to a certain extent, and thus is more robust to different TLS point cloud quality and shrub canopy architecture. In this study, the standard deviation of height was selected as the optimal height metric of AGB prediction, indicating that the canopy volume is more sensitive to the variability in canopy internal structure for individual *C. microphylla* than height. Meanwhile, a larger grid size of 7 cm, rather than the smallest 1 cm, yielded the most reliable indicator of individual shrub AGB, which in turn reflected the relatively sparse distribution of individual canopy structure for *C. microphylla*. In addition, the surface differencing method may be easier to transfer from the TLS data to UAV-LiDAR data,

especially in short canopies and even-distributed ecosystems (Greaves et al., 2015). Nonetheless, the relatively low point cloud density and the underestimated canopy height error (RMSE = 0.23 m, Fig. S3) for UAV-based LiDAR limits its ability to accurately capture the full canopy volume of individual shrubs, resulting in an extended grid size and weak estimation accuracy of individual shrub AGB (Fig. S4).

The remotely sensed estimation of vegetation biomass is typically calibrated with destructive harvesting data (Cooper et al., 2017; Li et al., 2015). However, destructive harvesting limits the in-depth ecological study on the pattern and change of shrub encroachment. Our results demonstrate that TLS model could achieve a higher accuracy than UAV model, supporting the potential of TLS as an alternative of destructive harvest.

This study provides an applicable workflow for wall-to-wall measurement of individual shrub AGB using the combination of UAV-based high-resolution optical sensors and TLS without destructive harvesting. Additionally, in our study area, *C. microphylla* is the only shrub species, and the other two dominant species are herbs, which are not considered in current study. For multi-species areas, our method could expand to a species-specific AGB estimation model with TLS, if the species of individual shrubs could be accurately identified by improving classification algorithms. It is also important to predict herb biomass, further exploring shrub-grass interactions and understanding the causes, ecological process and consequences of shrub encroachment.

6. Conclusions

In this study we estimated and mapped the individual shrub AGB using the UAV-based multispectral and LiDAR data with the nondestructive calibration by the terrestrial LiDAR in a shrub-encroached grassland in Inner Mongolia, China. By identifying individual shrubs, we determined the dominant textural, volumetric, geometric and spectral indicators of individual shrub AGB. Even though the combination of multispectral and LiDAR data obtained the best prediction accuracy of individual shrub AGB, the high-resolution multispectral imagery shows greater potential due to its high cost effectiveness and reliable accuracy. Furthermore, by the semi-automatic processing and the use of a UAV-based platform, the temporal resolution is no longer limited to snapshot observations (e.g. once a year or less) with the inclusion of beneficial seasonal states of encroached shrubs. With the combination of ecological studies, our study would contribute to improving our understanding of the causes and consequences of shrub encroachment, and its effect on ecosystem structure and functioning in arid and semiarid grasslands.

CRediT authorship contribution statement

Yujin Zhao: Conceptualization, Methodology, Investigation, Writing - original draft. **Xiaoliang Liu:** Investigation, Writing - original draft. **Yang Wang:** Investigation, Writing - original draft. **Zhaoju Zheng:** Writing - original draft. **Shuxia Zheng:** Writing - original draft. **Dan Zhao:** Investigation. **Yongfei Bai:** Conceptualization, Writing - original draft, Writing - review & editing, Supervision, Funding acquisition.

Declaration of Competing Interest

The authors declare that they have no known competing financial interests or personal relationships that could have appeared to influence the work reported in this paper.

Acknowledgements

This work was supported by the National Key R&D Program of China (2016YFC0500801 and 2016YFC0500804) and National Natural Science Foundation of China (41801230). The authors appreciate the anonymous reviewers for constructive comments on our manuscript.

Appendix A. Supplementary material

Supplementary data to this article can be found online at https://doi.org/10.1016/j.jag.2021.102358.

References

Adhikari, A., Yao, J., Sternberg, M., Mcdowell, K., White, J.D., 2017. Aboveground biomass of naturally regenerated and replanted semi-tropical shrublands derived from aerial imagery. Landscape Ecol. Eng. 13, 145–156.
Almeida, C.T.d., Galvão, L.S., Aragão, L.E.d.O.C.e., Ometto, J.P.H.B., Jacon, A.D., Pereira, F.R.d.S., Sato, L.Y., Lopes, A.P., Graça, P.M.L.d.A., Silva, C.V.d.J., Ferreira-Ferreira, J., Longo, M., 2019. Combining LiDAR and hyperspectral data for aboveground biomass modeling in the Brazilian Amazon using different regression algorithms. Remote Sensing Environ. 232, 111323–111323.
Asner, G.P., Martin, R.E., 2009. Airborne spectranomics: mapping canopy chemical and taxonomic diversity in tropical forests. Front. Ecol. Environ. 7, 269–276.
Bazezew, M.N., Hussin, Y.A., Kloosterman, E.H., 2018. Integrating Airborne LiDAR and Terrestrial Laser Scanner forest parameters for accurate above-ground biomass/carbon estimation in Ayer Hitam tropical forest, Malaysia. Int. J. Appl. Earth Obs. Geoinf. 73, 638–652.
Berner, L.T., Jantz, P., Tape, K.D., Goetz, S.J., 2018. Tundra plant above-ground biomass and shrub dominance mapped across the North Slope of Alaska. Environ. Res. Lett. 13, 035002.
Breiman, L., 2001. Random forests. Machine Learn. 45, 5–32.
Brovelli, M.A., Crespi, M., Fratarcangeli, F., Giannone, F., Realini, E., 2008. Accuracy assessment of high resolution satellite imagery orientation by leave-one-out method. ISPRS-J. Photogramm. Remote Sens. 63, 427–440.
Cao, J., Leng, W., Liu, K., Liu, L., He, Z., Zhu, Y., 2018. Object-based mangrove species classification using unmanned aerial vehicle hyperspectral images and digital surface models. Remote Sensing 10, 89.
Caracciolo, D., Istanbulluoglu, E., Noto, L.V., Collins, S.L., 2016. Mechanisms of shrub encroachment into Northern Chihuahuan Desert grasslands and impacts of climate change investigated using a cellular automata model. Adv. Water Resour. 91, 46–62.
Chang, A., Eo, Y., Kim, Y., Kim, Y.I., 2013. Identification of individual tree crowns from LiDAR data using a circle fitting algorithm with local maxima and minima filtering. Remote Sensing Lett. 4, 29–37.
Chen, L.Y., Li, H., Zhang, P., Zhao, X., Zhou, L.H., Liu, T.Y., Hu, H.F., Bai, Y.F., Shen, H. H., Fang, J.Y., 2015. Climate and native grassland vegetation as drivers of the community structures of shrub-encroached grasslands in Inner Mongolia, China. Landscape Ecol. 30, 1627–1641.
Chen, W., Zhao, J., Cao, C., Tian, H., 2018. Shrub biomass estimation in semi-arid sandland ecosystem based on remote sensing technology. Global Ecol. Conserv. 16 https://doi.org/10.1016/j.gecco.2018.e00479.
Cooper, S., Roy, D., Schaaf, C., Paynter, I., 2017. Examination of the potential of terrestrial laser scanning and structure-from-motion photogrammetry for rapid nondestructive field measurement of grass biomass. Remote Sensing 9, 531.
Coops, N.C., Wulder, M.A., Culvenor, D.S., Stonge, B., 2004. Comparison of forest attributes extracted from fine spatial resolution multispectral and lidar data. Can. J. Remote Sensing 30, 855–866.
Cunliffe, A.M., Brazier, R.E., Anderson, K., 2016. Ultra-fine grain landscape-scale quantification of dryland vegetation structure with drone-acquired structure-from-motion photogrammetry. Remote Sensing Environ. 183, 129–143.
Eisfelder, C., Kuenzer, C., Dech, S., 2011. Derivation of biomass information for semi-arid areas using remote-sensing data. Int. J. Remote Sens. 33, 2937–2984.
Eldridge, D.J., Bowker, M.A., Maestre, F.T., Roger, E., Reynolds, J.F., Whitford, W.G., 2011. Impacts of shrub encroachment on ecosystem structure and functioning: towards a global synthesis. Ecol. Lett. 14, 709–722.
Forsmoo, J., Anderson, K., Macleod, C., Wilkinson, M., Brazier, R., 2018. Drone-based structure-from-motion photogrammetry captures grassland sward height variability. J. Appl. Ecol. 55, 2587–2599.
Gessner, U., Machwitz, M., Conrad, C., Dech, S., 2013. Estimating the fractional cover of growth forms and bare surface in savannas. A multi-resolution approach based on regression tree ensembles. Remote Sens. Environ. 129, 90–102.
Goslee, S.C., Havstad, K.M., Peters, D.P.C., Rango, A., Schlesinger, W.H., 2003. High-resolution images reveal rate and pattern of shrub encroachment over six decades in New Mexico, U.S.A. J. Arid Environ. 54, 755–767.
Greaves, H.E., Vierling, L.A., Eitel, J.U.H., Boelman, N.T., Magney, T.S., Prager, C.M., Griffin, K.L., 2015. Estimating aboveground biomass and leaf area of low-stature Arctic shrubs with terrestrial LiDAR. Remote Sens. Environ. 164, 26–35.
Greaves, H.E., Vierling, L.A., Eitel, J.U.H., Boelman, N.T., Magney, T.S., Prager, C.M., Griffin, K.L., 2016. High-resolution mapping of aboveground shrub biomass in Arctic tundra using airborne lidar and imagery. Remote Sens. Environ. 184, 361–373.
Greaves, H.E., Vierling, L.A., Eitel, J.U.H., Boelman, N.T., Magney, T.S., Prager, C.M., Griffin, K.L., 2017. Applying terrestrial lidar for evaluation and calibration of airborne lidar-derived shrub biomass estimates in Arctic tundra. Remote Sensing Lett. 8, 175–184.
Guo, Z.C., Wang, T., Liu, S.L., Kang, W.P., Chen, X., Feng, K., Zhang, X.Q., Zhi, Y., 2021. Biomass and vegetation coverage survey in the Mu Us sandy land - based on unmanned aerial vehicle RGB images. Int. J. Appl. Earth Obs. Geoinf. 94, 102239.
Haralick, R.M., Shanmugam, K., Dinstein, I., 1973. Textural features for image classsification. Ieee Trans. Syst. Man Cybernetics SMC3, 610–621.

Jetz, W., Cavender-Bares, J., Pavlick, R., Schimel, D., Davis, F.W., Asner, G.P., Guralnick, R., Kattge, J., Latimer, A.M., Moorcroft, P., 2016. Monitoring plant functional diversity from space. Nat. Plants 2, 16024.
Jones, M., Allred, B., Naugle, D., Maestas, J., Donnelly, P., Metz, L., Karl, J., Smith, R., Bestelmeyer, B., Boyd, C., Kerby, J., McIver, J., 2018. Innovation in rangeland monitoring: annual, 30 m, plant functional type percent cover maps for U.S. rangelands, 1984-2017. Ecosphere 9, e02430.
Kalacska, M., Chmura, G.L., Lucanus, O., Bérubé, D., Arroyo-Mora, J.P., 2017. Structure from motion will revolutionize analyses of tidal wetland landscapes. Remote Sens. Environ. 199, 14–24.
Kelsey, K., Neff, J., 2014. Estimates of aboveground biomass from texture analysis of landsat imagery. Remote Sensing 6, 6407–6422.
Ku, N.W., Popescu, S.C., 2019. A comparison of multiple methods for mapping local-scale mesquite tree aboveground biomass with remotely sensed data. Biomass Bioenergy 122, 270–279.
Laliberte, A.S., Rango, A., Havstad, K.M., Paris, J.F., Beck, R.F., McNeely, R., Gonzalez, A.L., 2004. Object-oriented image analysis for mapping shrub encroachment from 1937 to 2003 in southern New Mexico. Remote Sens. Environ. 93, 198–210.
Li, A., Glenn, N.F., Olsoy, P.J., Mitchell, J.J., Shrestha, R., 2015. Aboveground biomass estimates of sagebrush using terrestrial and airborne LiDAR data in a dryland ecosystem. Agric. For. Meteorol. 213, 138–147.
Li, H., Shen, H.H., Chen, L.Y., Liu, T.Y., Hu, H.F., Zhao, X., Zhou, L.H., Zhang, P.J., Fang, J.Y., 2016a. Effects of shrub encroachment on soil organic carbon in global grasslands. Sci. Rep. 6, 9.
Li, W., Buitenwerf, R., Munk, M., Amoke, I., Bcher, P.K., Svenning, J.C., 2020c. Accelerating savanna degradation threatens the Maasai Mara socio-ecological system. Global Environ. Change 60, 102030.
Li, W., Buitenwerf, R., Munk, M., Bcher, P.K., Svenning, J.C., 2020a. Deep-learning based high-resolution mapping shows woody vegetation densification in greater Maasai Mara ecosystem. Remote Sens. Environ. 247, 111953.
Li, W., Niu, Z., Chen, H., Li, D., Wu, M., Zhao, W., 2016b. Remote estimation of canopy height and aboveground biomass of maize using high-resolution stereo images from a low-cost unmanned aerial vehicle system. Ecol. Ind. 67, 637–648.
Li, W., Niu, Z., Shang, R., Qin, Y., Chen, H., 2020b. High-resolution mapping of forest canopy height using machine learning by coupling ICESat-2 LiDAR with Sentinel-1, Sentinel-2 and Landsat-8 data. Int. J. Appl. Earth Obs. Geoinf. 92, 102163.
Lu, D., 2007. The potential and challenge of remote sensing-based biomass estimation. Int. J. Remote Sens. 27, 1297–1328.
Ludwig, A., Meyer, H., Nauss, T., 2016. Automatic classification of Google Earth images for a larger scale monitoring of bush encroachment in South Africa. Int. J. Appl. Earth Obs. Geoinf. 50, 89–94.
Madsen, B., Treier, U.A., Zlinszky, A., Lucieer, A., Normand, S., 2020. Detecting shrub encroachment in seminatural grasslands using UAS LiDAR. Ecol. Evol. 10, 4876–4902.
Maimaitijiang, M., Sagan, V., Sidike, P., Maimaitiyiming, M., Hartling, S., Peterson, K.T., Maw, M.J.W., Shakoor, N., Mockler, T., Fritschi, F.B., 2019. Vegetation Index Weighted Canopy Volume Model (CVMVI) for soybean biomass estimation from Unmanned Aerial System-based RGB imagery. ISPRS J. Photogramm. Remote Sens. 151, 27–41.
Meng, S.L., Pang, Y., Zhang, Z.J., Jia, W., Li, Z.Y., 2016. Mapping aboveground biomass using texture indices from aerial photos in a temperate forest of northeastern China. Remote Sensing 8, 230.
Nichol, J.E., Sarker, M.L.R., 2011. Improved biomass estimation using the texture parameters of two high-resolution optical sensors. IEEE Trans. Geosci. Remote Sens. 49, 930–948.
Nystrom, M., Holmgren, J., Olsson, H., 2012. Prediction of tree biomass in the forest-tundra ecotone using airborne laser scanning. Remote Sens. Environ. 123, 271–279.
Olsoy, P.J., Glenn, N.F., Clark, P.E., 2014. Estimating sagebrush biomass using terrestrial laser scanning. Rangeland Ecol. Manage. 67, 224–228.
Peng, H., Li, X., Li, G., Zhang, Z., Zhang, S., Li, L., Zhao, G., Jiang, Z., Ma, Y., 2013. Shrub encroachment with increasing anthropogenic disturbance in the semiarid Inner Mongolian grasslands of China. Catena 109, 39–48.
Prosek, J., Simova, P., 2019. UAV for mapping shrubland vegetation: Does fusion of spectral and vertical information derived from a single sensor increase the classification accuracy? Int. J. Appl. Earth Obs. Geoinf. 75, 151–162.
Riaño, D., Chuvieco, E., Ustin, S.L., Salas, J., Rodríguez-Pérez, J.R., Ribeiro, L.M., Viegas, D.X., Moreno, J.M., Fernández, H., 2007. Estimation of shrub height for fuel-type mapping combining airborne LiDAR and simultaneous color infrared ortho imaging. Int. J. Wildland Fire 16, 341–348.
Riegel, J.B., Bernhardt, E., Swenson, J., 2013. Estimating above-ground carbon biomass in a newly restored coastal plain wetland using remote sensing. PLoS ONE 8, e68251.
Roques, K., O'connor, T., Watkinson, A.R., 2001. Dynamics of shrub encroachment in an African savanna: relative influences of fire, herbivory, rainfall and density dependence. J. Appl. Ecol. 38, 268–280.
Sarker, L.R., Nichol, J.E., 2011. Improved forest biomass estimates using ALOS AVNIR-2 texture indices. Remote Sens. Environ. 115, 968–977.
Sheridan, R.D., Popescu, S.C., Gatziolis, D., Morgan, C.L.S., Ku, N.W., 2015. Modeling forest aboveground biomass and volume using airborne LiDAR metrics and forest inventory and analysis data in the pacific northwest. Remote Sensing 7, 229–255.
Strand, E.K., Smith, A.M.S., Bunting, S.C., Vierling, L.A., Hann, D.B., Gessler, P.E., 2006. Wavelet estimation of plant spatial patterns in multitemporal aerial photography. Int. J. Remote Sensing 27, 2049–2054.
Streutker, D.R., Glenn, N.F., 2006. LiDAR measurement of sagebrush steppe vegetation heights. Remote Sens. Environ. 102, 135–145.
Strobl, C., Boulesteix, A.-L., Kneib, T., Augustin, T., Zeileis, A., 2008. Conditional variable importance for random forests. BMC Bioinf. 9, 307–307.
Suykens, J.A.K., Vandewalle, J., 1999. Least squares support vector machine classifiers. Neural Process. Lett. 9, 293–300.
Teng, G.E., Zhou, M., Li, C., Wu, H., Li, W., Meng, F., Zhou, C., Ma, L., 2017. Mini-UAV LiDAR for power line inspection. ISPRS - International Archives of the Photogrammetry, Remote Sensing and Spatial Information Sciences, pp. 297–300.
Van Auken, O.W., 2009. Causes and consequences of woody plant encroachment into western North American grasslands. J. Environ. Manage. 90, 2931–2942.
Vierling, L.A., Xu, Y., Eitel, J.U.H., Oldow, J.S., 2012. Shrub characterization using terrestrial laser scanning and implications for airborne LiDAR assessment. Can. J. Remote Sensing 38, 709–722.
Wallace, L., Hillman, S., Reinke, K., Hally, B., Kriticos, D., 2017. Non-destructive estimation of above-ground surface and near-surface biomass using 3D terrestrial remote sensing techniques. Methods Ecol. Evol. 8, 1607–1616.
Wijesingha, J., Moeckel, T., Hensgen, F., Wachendorf, M., 2018. Evaluation of 3D point cloud-based models for the prediction of grassland biomass. Int. J. Appl. Earth Obs. Geoinf. 78, 352–359.
Xu, M., Cao, C., Tong, Q., Li, Z., Zhang, H., He, Q., Gao, M., Zhao, J., Zheng, S., Chen, W., 2010. Remote sensing based shrub above-ground biomass and carbon storage mapping in Mu Us desert, China. Sci. China Technol. Sci. 53, 176–183.
Yamashita, T., Yamashita, K., Kamimura, R., 2007. A stepwise AIC method for variable selection in linear regression. Commun. Stat.-Theory Methods 36, 2395–2403.
Zahawi, R.A., Dandois, J.P., Holl, K.D., Nadwodny, D., Reid, J.L., Ellis, E.C., 2015. Using lightweight unmanned aerial vehicles to monitor tropical forest recovery. Biol. Conserv. 186, 287–295.
Zandler, H., Brenning, A., Samimi, C., 2015a. Potential of space-borne hyperspectral data for biomass quantification in an arid environment: advantages and limitations. Remote Sensing 7, 4565–4580.
Zandler, H., Brenning, A., Samimi, C., 2015b. Quantifying dwarf shrub biomass in an arid environment: comparing empirical methods in a high dimensional setting. Remote Sens. Environ. 158, 140–155.
Zhang, S., Zhao, Y.J., Bai, Y.F., Yang, L., Sun, Z.Y., 2019. Remote sensing identification of grassland shrubs using low-altitude unmanned aerial vehicles. Tropical Geogr. 39, 512–520 (in Chinese).
Zhang, Z., Wang, S.P., Nyren, P., Jiang, G.M., 2006. Morphological and reproductive response of Caragana microphylla to different stocking rates. J. Arid Environ. 67, 671–677.
Zhao, D., Pang, Y., Li, Z., Sun, G., 2013. Filling invalid values in a lidar-derived canopy height model with morphological crown control. Int. J. Remote Sens. 34, 4636–4654.
Zhao, Y.J., Zeng, Y., Zhao, D., Wu, B.F., Zhao, Q.J., 2016. The optimal leaf biochemical selection for mapping species diversity Based on imaging spectroscopy. Remote Sensing 8, 216.
Zhou, L.H., Shen, H.H., Chen, L.Y., Li, H., Zhang, P.J., Zhao, X., Liu, T.Y., Liu, S.S., Xing, A.J., Hu, H.F., Fang, J.J., 2019. Ecological consequences of shrub encroachment in the grasslands of northern China. Landscape Ecol. 34, 119–130.
Zhou, Y., Chen, J., Chen, X.H., Cao, X., Zhu, X.L., 2013. Two important indicators with potential to identify Caragana microphylla in xilin gol grassland from temporal MODIS data. Ecol. Ind. 34, 520–527.